The Astrophysical Journal, 979:82 (12pp), 2025 January 20 https://doi.org/10.3847/1538-4357/ad9d37

Detecting the Black Hole Candidate Population in M51's Young Massive Star Clusters: Constraints on Accreting Intermediate-mass Black Holes

Kristen C. Dage[1], Evangelia Tremou[2], Bolivia Cuevas Otahola[3], Eric W. Koch[4], Kwangmin Oh[5], Richard M. Plotkin[6,7], Vivian L. Tang[8], Muhammad Ridha Aldhalemi[9], Zainab Bustani[9], Mariam Ismail Fawaz[9], Hans J. Harff[9], Amna Khalyleh[9], Timothy McBride[9], Jesse Mason[9], Anthony Preston[9], Cortney Rinehart[9], Ethan Vinson[9], Gemma Anderson[1], Edward M. Cackett[10], Shih Ching Fu[1], Sebastian Kamann[11], Teresa Panurach[12], Renuka Pechetti[11], Payaswini Saikia[13], Susmita Sett[1], Ryan Urquhart[5], and Christopher Usher[14]
[1] International Centre for Radio Astronomy Research—Curtin University, GPO Box U1987, Perth, WA 6845, Australia; kristen.dage@curtin.edu.au
[2] National Radio Astronomy Observatory, Socorro, NM 87801, USA
[3] Departamento de Matemáticas-FCE, Benemérita Universidad Autónoma de Puebla, Puebla, 72000, Mexico
[4] Center for Astrophysics | Harvard & Smithsonian, 60 Garden Street, Cambridge, MA 02138, USA
[5] Center for Data Intensive and Time Domain Astronomy, Department of Physics and Astronomy, Michigan State University, East Lansing, MI 48824, USA
[6] Department of Physics, University of Nevada, Reno, NV 89557, USA
[7] Nevada Center for Astrophysics, University of Nevada, Las Vegas, NV 89154, USA
[8] Department of Astronomy & Astrophysics, University of California, 1156 High Street, Santa Cruz, CA 95064, USA
[9] Henry Ford College, 5101 Evergreen Rd, Dearborn, MI 48128, USA
[10] Department of Physics & Astronomy, Wayne State University, 666 W. Hancock Sreet, Detroit, MI 48201, USA
[11] Astrophysics Research Institute, Liverpool John Moores University, IC2 Liverpool Science Park, 146 Brownlow Hill, Liverpool, L3 5RF, UK
[12] Center for Materials Research, Department of Physics, Norfolk State University, Norfolk VA 23504, USA
[13] Center for Astro, Particle and Planetary Physics, New York University Abu Dhabi, PO Box 129188, Abu Dhabi, UAE
[14] The Oskar Klein Centre, Department of Astronomy, Stockholm University, AlbaNova, SE-106 91 Stockholm, Sweden
Received 2024 October 31; revised 2024 December 4; accepted 2024 December 9; published 2025 January 20

Abstract

Intermediate-mass black holes ($10^2 < M_{\rm BH} < 10^5 M_\odot$) are an open question in our understanding of black hole evolution and growth. They have long been linked to dense star cluster environments, thanks to cluster dynamics, but there are a limited number of secure detections. We leverage existing X-ray observations from the Chandra X-ray Observatory and optical catalogs from the Hubble Space Telescope (HST) as well as new radio observations from the Karl G. Jansky Very Large Array to search for any evidence of accreting black holes in young massive star clusters in the nearby galaxy M51. We find that of 44 bright ($L_{\rm X} > 10^{38}$ erg s^{-1}) X-ray point sources in M51, 24 had probable matches to objects including possible associated star clusters in the HST Legacy Extragalactic UV Survey catalog, seven of which were classified as contaminants (background galaxies or foreground stars). We explore the optical properties of the remaining 17 sources, including cluster age and mass estimates, and search for radio counterparts in the 8–12 GHz band. The lack of radio counterparts to X-ray sources we know to be associated with young massive star clusters in M51 suggests that we do not significantly detect hard-state intermediate-mass black holes (IMBHs) $\sim 10^4\ M_\odot$ or above. However, more sensitive radio facilities, like the Square Kilometre Array and next-generation Very Large Array, may be able to provide evidence for IMBHs with masses down to $\sim 10^3\ M_\odot$.

Unified Astronomy Thesaurus concepts: Intermediate-mass black holes (816); Compact objects (288); Ultraluminous x-ray sources (2164); Young star clusters (1833); Star clusters (1567)

1. Introduction

Intermediate-mass black holes (IMBHs; $10^2 < M_{\rm BH} < 10^5\ M_\odot$) are a crucial stepping stone between stellar-mass BHs and the massive BHs observed at the centers of galaxies already at early cosmological epochs (E. Bañados et al 2018). One of the main theories for supermassive BH formation is that they are formed from the seeds of IMBHs, but the observational constraints on IMBHs are few, and their formation channels remain relatively unconstrained (J. E. Greene et al. 2020; A. Askar et al. 2023). Ultraluminous X-ray sources (ULXs; non-nuclear point sources whose X-ray luminosity exceeds the Eddington Limit for a 10 $M_\odot$ BH—around 10^{39} erg s^{-1}) have been seen as promising IMBH candidates, due to their unusually high X-ray luminosity (G. Fabbiano 1989), although most are likely an extreme form of a stellar-mass compact object accreting at super-Eddington rates (J. C. Gladstone et al. 2009 and references therein).

Our understanding of ULXs evolved significantly when X-ray pulsations were detected from M82-X2 (M. Bachetti et al. 2014)—the first of several observations to show that neutron stars could accrete well above their own Eddington limit. However, these pulsations are transient, which makes it difficult to rule out a neutron star primary from timing observations (M. Bachetti et al. 2014; S. N. Pike et al. 2019). We thus know that an observed X-ray luminosity of 10^{39} erg s^{-1} can be produced by a massive ($>10\ M_\odot$) BH accreting at a sub-Eddington rate or super-Eddington accretion onto a stellar-mass object, either a neutron star or a $<10\ M_\odot$ BH.

From the X-ray perspective, ULXs have almost exclusively been found outside the Milky Way, with most located in spiral galaxies (e.g., K. Kovlakas et al. 2020 and many references

therein). A small number of ULXs have been identified in globular clusters associated with elliptical galaxies (K. C. Dage et al. 2020 and references therein). While globular clusters were initially looked to as the natural birthplaces of IMBHs, radio studies like that of E. Tremou et al. (2018) have placed relatively stringent constraints on the presence of massive IMBHs in Galactic globular clusters, although the presence of IMBHs in systems like ω Cen and 47 Tuc is currently being debated (M. Häberle et al. 2024; T. Panurach et al. 2024 and references therein), and evidence for IMBHs has been found in tidally stripped nuclei (R. Pechetti et al. 2022 and references therein). By comparison, young massive star clusters (YMCs) remain fairly poorly studied.

Much theoretical work has also focused on the formation of BHs in YMCs—particularly the formation of IMBHs. YMCs are typically younger than globular clusters, with ages from 1 Myr to hundreds of megayears and masses greater than 10^4 $M_\odot$. They can, however, overlap in size with globular clusters (e.g., S. F. Portegies Zwart et al. 2010). As dense stellar environments, YMCs are conducive toward forming massive BHs via runaway stellar collisions and mergers, as shown by N-BODY simulations (e.g., S. F. Portegies Zwart & S. L. W. McMillan 2002; S. F. Portegies Zwart et al. 2004; M. Mapelli et al. 2008; M. Mapelli & L. Zampieri 2014; U. N. Di Carlo et al. 2019, 2021; S. Rastello et al. 2021).

However, unlike globular clusters, the observations of X-ray sources in YMCs are relatively sparser: B. Rangelov et al. (2011, 2012) found observational connections between star clusters and X-ray binaries (XRBs), in NGC 4449 and the Antennae galaxies, and some ULXs have been serendipitously identified in YMCs (such as Y. Terashima et al. 2006; P. K. Abolmasov et al. 2007; M. Heida et al. 2014; H. Avdan et al. 2016; K. M. López et al. 2017; R. Urquhart et al. 2018). Subsequent studies by B. A. Binder et al. (2023) and A. Akyuz et al. (2024) have targeted M31 and M33 as well as NGC 4490 and NGC 4214. B. A. Binder et al. (2023) found that while XRBs show spatial correlation with young star clusters, very few of the brightest XRBs are observed within the young star clusters. A. Akyuz et al. (2024) found that a high percentage of detected XRBs are associated with star clusters, with most being in the younger and less massive clusters. Q. Hunt et al. (2023) explored the connection between XRBs and star clusters in six star-forming galaxies, finding that the youngest XRBs hosting clusters in their sample were the more massive clusters.

The XRBs in all of these studies span a wide range in X-ray luminosity, from 10^{36} to 10^{39} erg s^{-1}, and may be an assortment of high-mass XRBs (HMXRBs), intermediate-mass XRBs, and low-mass XRBs (LMXRBs). From an observational perspective, it is not possible to classify the nature of the compact object from the X-ray luminosity alone; as previously discussed, neutron stars are able to achieve X-ray luminosities above 10^{39} erg s^{-1}, and the same is true of stellar-mass BHs (J. C. Gladstone et al. 2009). However, this is an area where radio follow-up may be able to differentiate between a stellar-mass accretor and a more massive one. Radio observations of ULXs are key to determining whether the accretor is an IMBH or a stellar-mass neutron star or BH (M. Mezcua et al. 2013, 2015; T. Panurach et al. 2024). If a 10^4 $M_\odot$ IMBH ($L_X \approx 10^{39}$–10^{40} erg s^{-1}) is accreting at a very low Eddington ratio ($<0.01L_{Edd}$), it could launch a compact radio jet, as observed from other low-luminosity active galactic nuclei (L. C. Ho 2008), using the fundamental plane of BH activity set forth in A. Merloni et al. (2003) and H. Falcke et al. (2004). The fundamental plane of BH activity is a nonlinear empirical relationship observed in both hard-state stellar-mass BHs and their supermassive counterparts, linking the X-ray (or nuclear [O III] emission-line) luminosity, compact radio luminosity, and the mass of the BH, demonstrating a consistent connection across vastly different BH scales (A. Merloni et al. 2003; H. Falcke et al. 2004; P. Saikia et al. 2015, 2018).

At the distances of nearby galaxies like M51 ($D < 10$ Mpc), the jetted radio emission from IMBHs can be readily observed by the Karl G. Jansky Very Large Array (VLA; R. A. Perley et al. 2011). We take advantage of the wealth of archival Chandra (M. C. Weisskopf et al. 2002) X-ray observations of the high-star-formation-rate spiral galaxy M51, known to host a multitude of ULXs and other X-ray-bright sources, along with the publicly available star cluster catalogs from the Hubble Space Telescope (HST) Legacy Extragalactic UV Survey (LEGUS; D. Calzetti et al. 2015; A. Adamo et al. 2017) and new radio observations from the VLA to assess whether any of the XRBs associated with YMCs could possibly be IMBHs more massive than 10^4 $M_\odot$. We will be focusing on the brightest X-ray sources in M51 ($L_X > 10^{38}$ erg s^{-1} if at the distance of M51—8.58 Mpc; K. B. W. McQuinn et al. 2016). We perform Bayesian crossmatching analysis between the X-ray and optical using NWAY (M. Salvato et al. 2018) and compare our observations to state-of-the-art simulations of young star clusters. We also discuss what range of IMBH masses are actually observable in X-ray and radio at the distance of M51, given current observational facilities.

2. Data and Analysis

We combine multiwavelength observations from Chandra and HST by performing a Bayesian crossmatch between Chandra X-ray point sources and optical catalogs from LEGUS,[15] then search for a radio counterpart from the VLA to any X-ray-bright ($L_X > 10^{38}$ erg s^{-1}) sources with a candidate cluster optical counterpart. There are a number of caveats associated with our process and we list them below. However, despite the many challenges, our intention is to determine the maximum number of potential accreting IMBHs in star clusters to provide useful benchmarks to compare theory to, and thus we present all probabilities and caveats to probe both the optimistic and the realistic scenarios.

2.1. X-Ray Analysis

M51 has been studied in X-ray by Chandra 23 times in the last 21 yr, covering several different fields of the galaxy, spanning about 4.′5. We did initial crossmatching with the Chandra Source Catalog (CSC) V. 2.0 (I. N. Evans et al. 2010) to have a reasonably complete catalog of the entire field. We note that the CSC did have some (about 1%) spurious detections at the lower-luminosity ends, and the reported flux values differ from published detailed spectroscopic studies, perhaps due to the innate variability of some of the sources or assumptions about spectral shape.[16] For the brightest sources, we obtain X-ray luminosities and spectral parameters from existing long-term studies of M51's XRBs that perform detailed X-ray spectroscopy (T. Sanatombi et al. 2023). To

[15] https://legus.stsci.edu/
[16] https://cxc.cfa.harvard.edu/csc/caveats.html

target the faintest detectable XRBs, we run source detection and flux estimation on the longest-available observation.

To supplement the findings of the CSC and T. Sanatombi et al. (2023) on M51's brightest X-ray sources, we processed the longest-available observations of M51, ObsIDs 13812 (2012 September 12; 160 ks), 13813 (2012 September 9; 180 ks), 18314 (2012 September 20; 190 ks), 13815 (2012 September 23; 68 ks), and 13816 (2012 September 26; 74 ks) observed in 2012 (PI: Kuntz). The observations from 2012 are much longer than any other available observations and are useful for finding X-ray sources at the faintest detection limit, for the sake of completeness. For this analysis, we used the Chandra Interactive Analysis of Observations (CIAO, version 4.15.1; A. Fruscione et al. 2006), with the latest calibration files from the Chandra Calibration Database. We reprocessed all the data using `chandra_repro` and merged them with the `merge_obs` tool.

While we cannot perform detailed spectroscopy due to the low number of source counts (<10), nor trace the long-term X-ray behavior of the faint sources, we use `wavdetect` to identify fainter X-ray sources down to $L_X \sim 10^{37}$ erg s^{-1}. We used a range of spatial scales of 2, 4, 8, 16, 24, 32, and 48 pixels, with a significance threshold of 10^{-6}. This corresponds to about one false alarm per 1024 × 1024 pixel image. We computed unabsorbed X-ray fluxes using the `srcflux` tool, probing the 0.3–10.0 keV energy range. We assumed a hydrogen column density of 3.8×10^{18} cm^{-2}, which we obtained from H. Yu et al. (2023). We assumed a fixed power-law model, with a photon index of 1.7, and focused on the full 0.3–10.0 keV energy band to be consistent with T. Sanatombi et al. (2023). Details of the X-ray and star cluster properties are given in Table 1.

Table 1
Age and Mass Estimates of Cluster Candidates, along with Peak X-Ray Luminosity as Reported by T. Sanatombi et al. (2023) and Their Characteristic Best-fit X-Ray Spectral Shapes (Determined by the Model with the Best-fit Statistics over Most Observations—"DB" for a Disk Blackbody Best Fit and "PL" for a Power-law Model Best Fit)

ID	Age (yr)	Mass ($M_\odot$)	p_i (%)	Peak L_X (erg s^{-1})	Variable	X-Ray Spectrum
src03*	<1e6	<84	100	1.44×10^{38}	*M*	DB
src04	1e8	1542	39	7.24×10^{38}	*M*	PL
src12	2e8	17800	100	5.12×10^{38}	*t*	PL
src16	4e6	10670	35	1.22×10^{39}	*N*	PL
src17	<1e6	<84	59	6.02×10^{38}	*N*	DB
src18	1e6	650.7	30	6.91×10^{40}	*M*	DB
src19	7e8	19450	30	9.77×10^{38}	*N*	PL
src22	1e6	292	100	2.75×10^{38}	*N*	DB
src23	2e6	584	23	1.20×10^{40}	*M*	DB
src24	2e8	13930	100	1.02×10^{39}	*N*	DB?
src25 +	<1e6	<84	100	5.88×10^{39}	*M*	PL
src26 +	<1e6	<84	66	1.82×10^{39}	*H*	PL?
src28	3e6	230	100	2.19×10^{38}	*N*	PL
src31	2e6	1101	25	1.41×10^{39}	*H*	PL
src34	4e7	6107	100	3.47×10^{38}	*M*	DB?
src40	6e6	316	100	6.45×10^{38}	*t*	PL
src43	2e9	84860	100	1.20×10^{39}	*M*	DB?

Note. The "Variable" column has *t* for sources with only one X-ray detection in ObsID 1622—a 30 ks observation taken in 2001—that are not observed above the detection threshold in subsequent observations of equal or greater sensitivity, *N* for sources that do not vary significantly within their uncertainties, *M* for moderately variable sources (that vary within their uncertainties but not by an order of magnitude), and *H* for highly variable sources that vary by an order of magnitude. Src 25 and src26 are the eclipsing ULXs from R. Urquhart et al. (2018). Four sources did not have a mass or age estimate, so we assume the lowest age and mass estimates from the noncontaminated LEGUS list as upper limits on the ages and masses of these sources.

2.2. Star Cluster Catalog and Bayesian Crossmatching Analysis

According to the CSC, there are less than 200 X-ray point sources in a 5′ radius around M51. In a similarly sized region, LEGUS reports over 30,000 optical point sources. As detailed in Q. Hunt et al. (2023), the probability of chance superposition is certainly not negligible. By using NWAY[17] (M. Salvato et al. 2018), software designed for Bayesian crossmatching of multiple catalogs, we can provide some measure of constraint on the probability of the individual cluster candidate being a match to a given X-ray source, as NWAY computes the probability of a random chance alignment of two unrelated sources and folds this into the probability of association. NWAY reports two probabilities: p_any, the probability that there is a counterpart in the matching catalog; and p_i, the probability that a given source is an individual match. We only select sources with a high p_any (>0.5; M. Salvato et al. 2018). We report the highest p_i values; sources with a very high p_i had one close match within the uncertainty radius, and sources with lower p_i had multiple matches. We report all matches with p_i > 0.1, which show up as duplicate matches, e.g., in the cases of src98, src31, and src36.

Another word of caution about the crossmatching is that the LEGUS catalog of 30,000 objects is neither the full photometric list nor the full star-cluster-candidate catalog. It is a photometric list of any source with a concentration index (CI; see Section 2.3) greater than 1.35, with likely contaminants denoted. However, for our purposes, we are content to view the matches as the maximum number of X-ray sources that could possibly be matched to a cluster candidate.

We performed Bayesian crossmatching using NWAY to crossmatch the full LEGUS cluster candidate catalog and the CSC, with a maximum crossmatch radius of 1.″1. The full LEGUS catalog contains 30,176 objects. Of these, 10,925 met the cutoff to be considered for classification, with 7551 being class 4 contaminants, 385 being class 3 (compact stellar sources), and 2989 being class 1 or 2 clusters (most likely to be clusters). The remaining 19,251 objects are unclassified class 0 objects. These classifications are discussed in further detail in Section 2.3.

Thanks to T. Sanatombi et al. (2023), we were able to identify the brightest X-ray sources that are accompanied by detailed spectral modeling (both with a single power-law index and a single blackbody disk). Their analysis also includes the long-term properties of the source, to look for both variations in X-ray luminosity and X-ray spectral shape. We found that of the 43 bright X-ray sources in T. Sanatombi et al. (2023), 24 of them match a source in the LEGUS catalog. Of these, eight had high-probability matches with a class 4 object, and one was clearly a foreground star (src35).

NWAY, in addition to reporting the match probability, also provides match rankings, where, in the case of low-probability matches, other probable matches are also provided. For all of the cluster candidate sources (class 0, 1, 2, or 3) with match probabilities less than 50%, we examined the probability values and separations. All of the second-rank matches had much

[17] https://github.com/JohannesBuchner/nway

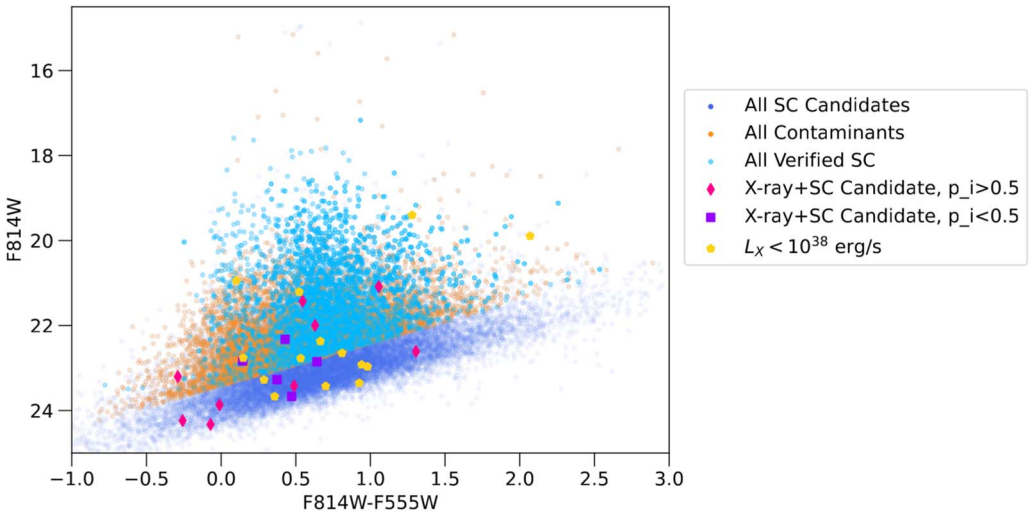

Figure 1. Color–magnitude diagram of all LEGUS cluster candidates, along with the verified star clusters (SCs) and contaminants. The yellow pentagons represent the X-ray sources matched to high-probability (>50%) matches to cluster candidates, lower-probability (<50%) matches to cluster candidates, or contaminants.

Table 2
Possible Matches between Bright X-Ray Sources in T. Sanatombi et al. (2023) and the LEGUS Catalog

ID	HST ID	R.A. and Decl.	F555W	F814W	CI	Cl1	Cl2	Sep. (arcsec)	p_i (%)
src03	2141	13:29:54.98 +47:09:23	23.97 ± 0.07	24.23 ± 0.20	1.7	0	2	0.14	100
src04	3060	13:29:47.48 +47:09:41	24.14 ± 0.13	23.67 ± 0.18	2.1	0	0	0.39	38
src08	7700	13:29:46.16 +47:10:42	23.37 ± 0.05	22.49 ± 0.07	1.6	4	4	0.47	30
src09	7494	13:29:53.31 +47:10:43	20.22 ± 0.05	21.57 ± 0.04	1.9	4	4	0.18	16
src09	7556	13:29:53.28 +47:10:43	19.16 ± 0.03	18.86 ± 0.03	1.5	2	2	0.54	13
src10	8391	13:29:57.61 +47:10:48	22.99 ± 0.06	22.57 ± 0.08	1.4	4	4	0.49	32
src12	8780	13:29:49.05 +47:10:55	21.97 ± 0.03	21.43 ± 0.04	1.7	1	1	0.83	100
src16	11819	13:29:53.56 +47:11:27	21.78 ± 0.03	21.15 ± 0.05	1.5	4	2	0.09	35
src17	12622	13:29:53.58 +47:11:33	22.91 ± 0.27	23.20 ± 0.45	2.0	0	0	0.55	59
src18	13341	13:29:43.31 +47:11:35	22.98 ± 0.04	22.83 ± 0.08	1.4	4	2	0.07	30
src19	13586	13:29:54.77 +47:11:36	22.75 ± 0.04	22.32 ± 0.18	1.8	4	2	0.34	30
src20	13003	13:29:54.23 +47:11:37	23.24 ± 0.20	22.76 ± 0.27	2.1	4	4	0.59	43
src21	14843	13:29:55.86 +47:11:45	22.41 ± 0.04	21.91 ± 0.05	2.0	4	4	0.25	28
src22	16025	13:29:45.6s +47:11:51	24.26 ± 0.06	24.33 ± 0.19	1.5	0	0	0.90	100
src23	16595	13:29:50.66 +47:11:55	23.65 ± 0.10	23.27 ± 0.12	1.6	0	0	0.40	22
src24	18061	13:29:57.65 +47:12:07	22.63 ± 0.03	21.99 ± 0.04	1.9	2	2	0.27	100
src25[a]	21034	13:29:39.96 +47:12:36	23.65 ± 0.04	23.85 ± 0.09	1.5	0	3	0.17	100
src26[a]	21770	13:29:39.46 +47:12:43	22.60 ± 0.03	22.53 ± 0.04	1.4	0	4	0.20	66
src28	22030	13:30:07.85 +47:12:46	23.86 ± 0.06	23.89 ± 0.12	1.4	0	2	0.62	100
src31	25510	13:30:04.32 +47:13:21	23.49 ± 0.06	22.85 ± 0.06	1.6	0	2	0.25	25
src31	30129	13:30:04.28 +47:13:21	23.12 ± 0.06	22.71 ± 0.06	1.4	4	4	0.36	24
src34	26467	13:29:58.36+47:13:32	23.92 ± 0.06	22.61 ± 0.06	1.7	0	2	0.61	100
src35	27115	13:29:38.64+47:13:36	15.50 ± 0.02	14.99 ± 0.03	2.1	0	4	0.18	100
src36	27626	13:30:00.99+47:13:44	23.38 ± 0.13	22.57 ± 0.12	1.5	4	4	0.20	12
src36	27620	13:30:00.98+47:13:44	23.22 ± 0.08	22.39 ± 0.06	1.8	3	4	0.31	12
src40	27137	13:29:56.20+47:14:51	23.91 ± 0.04	23.42 ± 0.06	1.5	0	2	0.45	100
src43	20431	13:29:57.46+47:16:11	22.14 ± 0.03	21.08 ± 0.04	1.5	1	1	0.41	100

Notes. The "ID" column refers to the ID assigned by T. Sanatombi et al. (2023), the "HST ID" is the ID assigned by the LEGUS catalog, and we provide the R.A. and decl. along with the F555W and F814W magnitudes and CI, from LEGUS. We also show the separation in arcseconds and the probability of an individual match as reported by NWAY. Src09, src31, and src36 have two different possible counterparts with nearly equal match probabilities and very similar distances. "CI" is the concentration index reported by LEGUS, and "p_i" is the individual match probability. "Cl1" indicates the LEGUS classification for the cluster candidate, and "Cl2" is our `nProFit` classification.
[a] Eclipsing ULX from R. Urquhart et al. (2018).

lower probability and were much farther in separation than the first-ranked matches, and we do not report them. The match probabilities, separations, source ID from T. Sanatombi et al. (2023), and properties measured by LEGUS are reported in Table 2. Figure 1 shows the color–magnitude diagram of the full LEGUS catalog, the verified star clusters, and the verified contaminants, along with the potential cluster matches to the bright X-ray sources. We also compare our stacked X-ray catalog, and Table 3 shows the low-X-ray-luminosity matches and cluster properties.

Table 3
X-Ray and Star Cluster Properties of Low-luminosity X-Ray Sources with High-probability Matches to Star Clusters

Chandra ID	HST ID	HST R.A. and Decl.	F555W	F814W	C.I.	Age (Myr)	Mass ($M_\odot$)	1	2	Sep. (arcsec)	p_i (%)	Sig.	L_X (10^{36} erg s^{-1})
2CXO J133001.4+471157	16982	13:30:01.37+47:11:57	23.70 ± 0.05	22.07 ± 0.05	1.5	<1	<84	0	3	0.71	100	9.0	$8.5^{+2.5}_{-3.3}$
2CXO J132942.0+471118	10925	13:29:42.10+47:11:19	23.46 ± 0.05	23.08 ± 0.05	1.4	400	6317	0	4	0.42	61	15.7	18.4 ± 3.4
2CXO J132953.9+470923	2135	13:29:53.95+47:09:23	21.84 ± 0.03	21.83 ± 0.04	1.6	<1	<84	0	4	0.45	100	11.7	$11.3^{+1.64}_{-2.04}$
2CXO J132940.9+471139	14091	13:29:40.84+47:11:39	22.91 ± 0.03	22.76 ± 0.05	1.6	<1	<84	0	2	0.81	100	12.8	15.0 ± 3.2
2CXO J132956.0+471350	28079	13:29:56.07+47:13:50	24.28 ± 0.06	23.36 ± 0.07	1.7	1	1400	0	2	0.26	100	13.1	$17.5^{+3.04}_{-3.46}$
2CXO J132955.3+471355	28421	13:29:55.30+47:13:55	23.86 ± 0.06	22.92 ± 0.06	1.7	200	6827	0	0	0.48	100	16.1	22.2 ± 3.7
2CXO J132958.7+471030	6559	13:29:58.72+47:10:30	23.60 ± 0.05	21.05 ± 0.04	1.6	<1	<84	0	3	0.20	69	19.4	18.2 ± 2.9
2CXO J132950.3+471322	25585	13:29:50.36+47:13:22	23.91 ± 0.06	22.74 ± 0.05	1.5	40	4301	0	4	0.46	100	18.8	28.1 ± 3.9
2CXO J132944.0+471156	16848	13:29:44.13+47:11:56	24.03 ± 0.08	23.67 ± 0.13	1.5	100	1878	0	0	0.56	50	21.1	27.2 ± 3.8
2CXO J132942.5+471042	7928	13:29:42.55 +47:10:43	23.56 ± 0.06	23.28 ± 0.12	1.4	200	4260	0	0	0.83	100	24.0	29.8 ± 4.1
2CXO J132952.7+471244	21961	13:29:52.72+47:12:45	23.99 ± 0.06	23.38 ± 0.09	1.5	10	316.7	0	4	0.68	100	30.6	40.8 ± 4.7
2CXO J132949.6+470910	1490	13:29:49.60+47:09:10	23.95 ± 0.06	22.97 ± 0.05	1.5	40	2663	0	2	0.14	70	31.2	35.7 ± 4.4
2CXO J132934.9+470934	2633	13:29:34.92+47:09:34	23.46 ± 0.06	22.65 ± 0.07	1.6	100	5092	0	0	0.51	100	29.2	52.8 ± 6.6
2CXO J133000.7+471212	18754	13:30:00.79+47:12:13	24.13 ± 0.06	23.43 ± 0.09	1.5	<1	<84	0	0	0.89	100	32.9	38.2 ± 4.3
2CXO J133004.0+471003	4772	13:30:04.08+47:10:03	23.30 ± 0.04	22.77 ± 0.04	1.7	<1	<84	0	0	0.21	67	37.2	40.2 ± 4.1
2CXO J133004.5+470949	3641	13:30:04.47+47:09:49	21.73 ± 0.03	21.21 ± 0.03	1.6	<1	<84	0	0	0.36	100	37.1	34.1 ± 3.9
2CXO J133010.0+471328	25879	13:30:10.04+47:13:27	21.96 ± 0.03	19.89 ± 0.03	1.8	3000	1081000	1	1	0.28	100	9.0	8.7 ± 2.5
2CXO J132937.9+470832	333	13:29:37.98+47:08:32	20.68 ± 0.02	19.40 ± 0.03	1.6	200	324500	1	1	0.31	55	29.8	108 ± 14.0
2CXO J132954.9+471102	9341	13:29:55.02+47:11:03	21.05 ± 0.03	20.95 ± 0.04	1.4	4	5456	1	1	0.83	100	34.4	39.8 ± 4.2
2CXO J132942.2+471046	8237	13:29:42.29+47:10:46	23.04 ± 0.04	22.37 ± 0.05	1.7	200	9632	2	2	0.66	100	23.9	29.8 ± 4.1

Note. X-ray luminosities and their significance from deep observations matched to the most probable noncontaminant matches in the LEGUS catalog. We exclude sources away from the galaxy center, as they have a higher probability of being background galaxies.

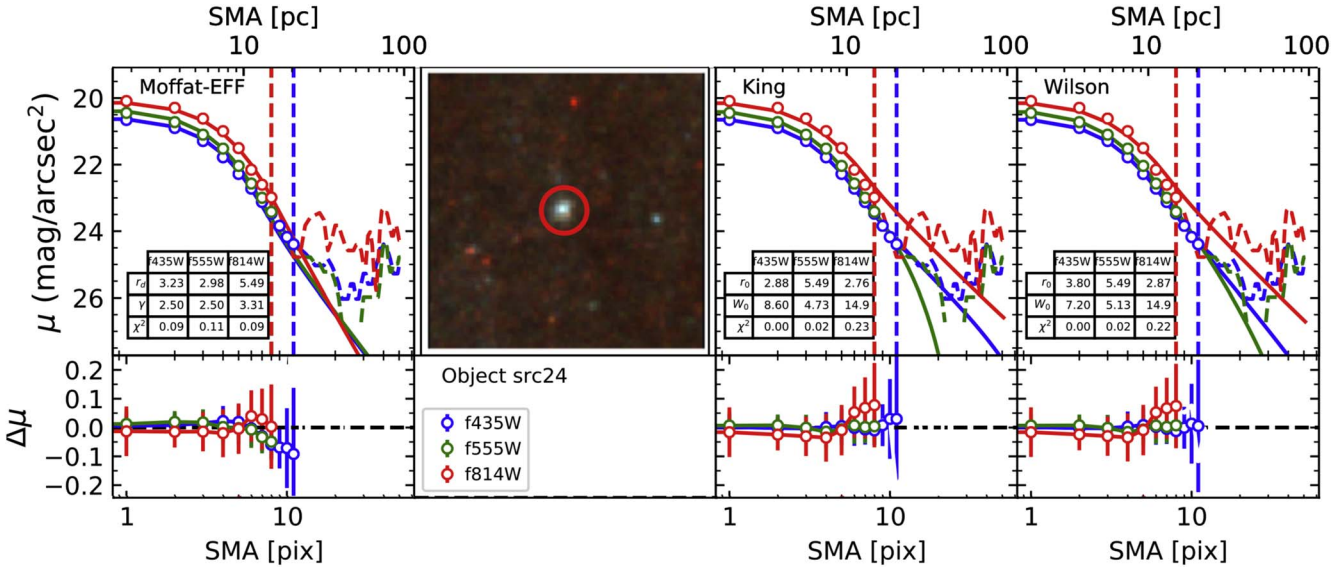

Figure 2. The SBPs of src24 in the F435W, F555W, and F814W HST observations are shown with the blue, green, and red empty circles, obtained by NPROFIT from isophotal fitting performed to the image centered at src24 coordinates (shown in the lower panels, from left to right). The SBPs are fitted using the Moffat-EFF (leftmost panel), King (third panel from left to right), and Wilson (rightmost panel) models, fitted to the SBPs up to the fitting radius shown with the vertical lines, following the same color-coding, with the minimum fitting radius between all bands shown as the circle in the snapshot in the second upper panel from left to right. The basic structural parameters obtained for each model are summarized in the inset tables. The bottom panels show the residuals of the dynamical model fits performed by NPROFIT.

According to the CSC, the absolute astrometric positional uncertainty at the 90% level is 1.″1.[18] As outlined in D. Calzetti et al. (2015), the World Coordinate System for the LEGUS images have been aligned to a WFC3/UVIS image, because the coordinates were derived from the more accurate Guide Star II catalog. While we are content to proceed with searching for matches within the 1.″1 positional uncertainty of Chandra, we want to emphasize that this search is on a population basis, and we recommend performing more detailed astrometry (e.g., K. Atapin et al. 2024) for any individual source of interest.

2.3. Young Star Cluster Classification and Star Cluster Structural Parameter Modeling

As detailed in A. Adamo et al. (2017), the young star cluster catalogs are obtained from HST observations in the following manner: the CI is calculated by obtaining the magnitude difference of each source at 1 and 3 pixel aperture radii to select out objects with more concentration of light from the rest. Their pipeline performs multiband photometry for these sources, along with averaged and CI-based aperture correction. To estimate the ages and masses of the clusters, the spectral energy distribution of each source is fitted with single-stellar-population models, both from the Padova and Geneva stellar libraries (C. Leitherer et al. 1999; G. A. Vázquez & C. Leitherer 2005). Three different types of internal extinction are applied: a Milky Way extinction law and two different types of starburst extinction models. We used the default reference catalog, which uses aperture-based correction, the Padova stellar library, and the Milky Way extinction. Cluster classification is based on a combination of both visual inspection by members of the team and machine learning, with classification quality flags being included in the full catalog. Classification is only performed on sources detected in at least four bands that are brighter than −6 V mag with photometric errors of 0.3 mag or less. Missed clusters are added back in at the visual inspection stage, typically below 1%. The flags are 0, 1, 2, 3, and 4, with 0 being unclassified sources and 4 being contaminants (including supernova remnants, foreground stars, background galaxies, and spurious detections). Class 1 and 2 sources are the most likely to be clusters, and class 3 sources are either less compact clusters or compact associations.

Only three of our bright X-ray sources matched to a class 1 or 2 source, and we found a low-probability match to a class 3 source (Table 2). The majority of our sources matched unclassified (class 0) star cluster candidates. For the rest of this analysis, we heavily emphasize that these are cluster candidates and that the masses and ages provided should be treated as estimates.

To ensure more secure cluster classification, we used the *n*-Profile Fitting tool `nProFit` (B. Cuevas-Otahola et al. 2022) to fit the observed surface brightness profiles (SBPs) of the cluster candidates described previously. `nProFit` is a publicly available code that enables fitting dynamical point-spread-function-convolved models (King, Wilson, and Moffat-EFF; I. R. King 1966; C. P. Wilson 1975; R. A. W. Elson et al. 1987) to the observed SBPs of star clusters. Such a procedure is carried out by `nProFit`, estimating and subtracting in the first place a local background value from images trimmed and centered at each cluster candidate position. Subsequently, the SBPs are extracted by `nProFit` from the background-subtracted images by means of isophotal fittings, which are performed considering the ellipticity values computed by `nProFit` in a previous iteration of the isophotal fitting. We show an example of the performed fits in Figure 2, where we illustrate the fitting of the Moffat-EFF, King, and Wilson models to src24, with Moffat-EFF being the best-fit model in the F814W band. Considering the obtained structural parameters, namely radii (r_0 or r_d) and shape (W_0 or γ) parameters, we assigned a classification to each cluster candidate, using the same flags as used in the LEGUS catalog (where, for us, 0 is too faint to fit properly, 1, 2, and 3 are

[18] https://cxc.harvard.edu/cal/ASPECT/celmon/

relatively compact, and 4 is extended), and compared both classifications. We found that our classification matches the LEGUS classification in 50% of cases. We highlight that we correctly identified the sources identified as clusters in LEGUS (src12, src24, and src43). In addition, we identified eight sources as compact and diffuse clusters, which were identified in LEGUS as spurious detections (src3, src16, src18, src19, src28, src31, src34, and src40). The rest of the clusters were identified as spurious sources or sources below the selection cut defined in LEGUS. For the rest of this analysis, we proceed with sources we classify as 1 or 2, and we also consider the ambiguous (class=0) cases.

2.4. Radio Data

Four quadrants of M51 were observed by the VLA observations between 2023 June and July (NRAO/VLA Program ID 23A-104; PI: K. Dage) in the most extended A-array configuration. The data were taken with *X*-band receivers (8–12 GHz). We used the 3 bit samplers, with two independent 2048 MHz wide basebands centered at 9.0 GHz and 11.0 GHz. The bandwidth was divided into 128 MHz wide spectral windows, and each spectral window was sampled by 64 channels. All observations were obtained in full polarization mode. Observations typically alternated between 6.5 minutes on target and 1 minutes on a phase calibrator (J1335+4542). 3C286 (1331+305) was observed at the start of each block as bandpass and flux calibrator. The total time of each observing block was 2 hr, with typically 1.1 hr on the source. Four different fields of M51 were targeted, centered at:

1. R.A.: $13^{h}29^{m}43\overset{s}{.}309$, decl.: $47°11'34\overset{''}{.}930$;
2. R.A.: $13^{h}30^{m}7\overset{s}{.}547$, decl.: $47°11'6\overset{''}{.}270$;
3. R.A.: $13^{h}30^{m}6\overset{s}{.}001$, decl.: $47°15'42\overset{''}{.}480$; and
4. R.A.: $13^{h}29^{m}50\overset{s}{.}656$, decl.: $47°11'55\overset{''}{.}206$, respectively.

The data were calibrated and imaged following standard procedures with the Common Astronomy Software Application (CASA; J. P. McMullin et al. 2007; CASA Team et al. 2022). A Briggs weighting scheme (robust=0; D. S. Briggs 1995) and frequency-dependent clean components (with two Taylor terms; nterms=2) were used in the imaging to mitigate large-bandwidth effects (U. Rau 2012). The mean rms noise of each primary-beam-corrected image was 4 μJy beam^{-1} and the median synthesized beam in the images is $0\overset{''}{.}16 \times 0\overset{''}{.}14$. This corresponds to a cutoff 3σ radio luminosity of 1.06×10^{34} erg s^{-1} at 10 GHz.

No significant radio counterpart was detected for any of the X-ray sources, except for the soft-X-ray source Src03, which had a nearby radio counterpart ($<1''$) that was 70 ± 8.4 μJy. For the sources not detected in radio or in the X-ray hard state, we can suggestively use these upper limits (beholden to the many assumptions underlying the fundamental plane) to exclude evidence for IMBHs of masses greater than 10^4 $M_\odot$. As outlined in T. Panurach et al. (2024), radio continuum detection is critical toward disentangling whether the X-ray emission could be produced by an IMBH, as evidence for radio jets would be observed.

3. Results and Discussion

We leveraged archival Chandra X-ray and HST optical observations of M51, along with new radio observations from the VLA. We found that of the 43 brightest X-ray sources in M51, 23 matched to cluster candidates in the LEGUS catalog, eight of which were contaminants. Of the remaining 15, three had high-probability matches to a classified star cluster, eight had high-probability matches to an unclassified star cluster candidate, and three had low-probability matches to a star cluster candidate. We also point out Src36, a known neutron star ULX (G. A. Rodrìguez Castillo et al. 2020), which had equally low-probability matches to a contaminant or an unclassified star cluster. After using `nProFit`, we conclude that neither potential optical counterpart is a star cluster. Overall, we found 24 bright X-ray sources possibly matching to an optical counterpart in the LEGUS catalog and 20 low-luminosity sources ($L_X < 10^{38}$ erg s^{-1}) with high-probability (>50%) individual matches.

An infrared study by K. M. López et al. (2017) suggests that Src09 may have a star cluster counterpart. In Table 2, we list the highest-probability match for Src09, which is a class 4 object, as well as the match probability and separation for the only classified cluster within the $1.1''$ radius (the third most distant match). If the cluster is the correct counterpart, the age would be 1 Myr and mass 42,260.0 $M_\odot$. However, we do not believe this is a probable match and do not include it in our analysis.

Y. Terashima et al. (2006) find that three of their ULXs may be in or near a star cluster. These correspond to Src09, Src26, Src36 in our nomenclature. They suggest a fourth source, corresponding to Src13, may be close to but unassociated with a star cluster. We do not find a statistically significant match within the $1\overset{''}{.}1$ radius between this source and anything in the full LEGUS catalog. We repeat the cautionary note from earlier that, on an individual basis, careful astrometry should be considered.

Given that our ultimate goal is to obtain the maximum possible number of accreting IMBHs to provide a benchmark to compare with a leading theory of the formation of massive BHs, despite the difficulties in determining optical counterparts in crowded fields, this crossmatching serves to act as a naive upper limit for comparison. However, we again caution against the use of any individual counterpart in further studies without performing careful astrometry.

With these caveats in mind, we found that most of the potential cluster candidate counterparts to bright X-ray sources in M51 had cluster masses less than 1000 $M_\odot$, four had masses between 1000 $M_\odot$ and 10,000 $M_\odot$, and three had masses over 10,000 $M_\odot$ (Figure 3). Nine are young, with ages less than 4 Myr, one has an age estimate of 6 Myr, four are between 40 and 200 Myr, and one is 2000 Myr (Figure 4).

The ages are significant; while it is well known that globular clusters do not have a dense intracluster medium (ICM; P. C. Freire et al. 2001), young clusters with ages <4 Myr may still have an ICM for a BH to accrete from. A number of studies—including N. Bastian & J. Strader (2014), K. Hollyhead et al. (2015), I. Cabrera-Ziri et al. (2015), and S. Hannon et al. (2019)—suggest that YMCs lose their gas within 2–4 Myr of their lives, so clusters up to 4 Myr may still have enough gas for a massive BH to accrete from, whereas the X-rays produced by the clusters older than 4 Myr must be due to accretion from a binary companion to the compact object. The fast clearing time is also consistent with the anticorrelation with 3.3 μm polycyclic aromatic hydrocarbon nondetection by M. J. Rodrìguez et al. (2023).

Notably, as shown in Figure 5, the majority of probable matches to clusters with ages less than 4 Myr are all to cluster candidates below 1000 $M_\odot$. The two most massive cluster candidate counterparts with ages less than 4 Myr and masses

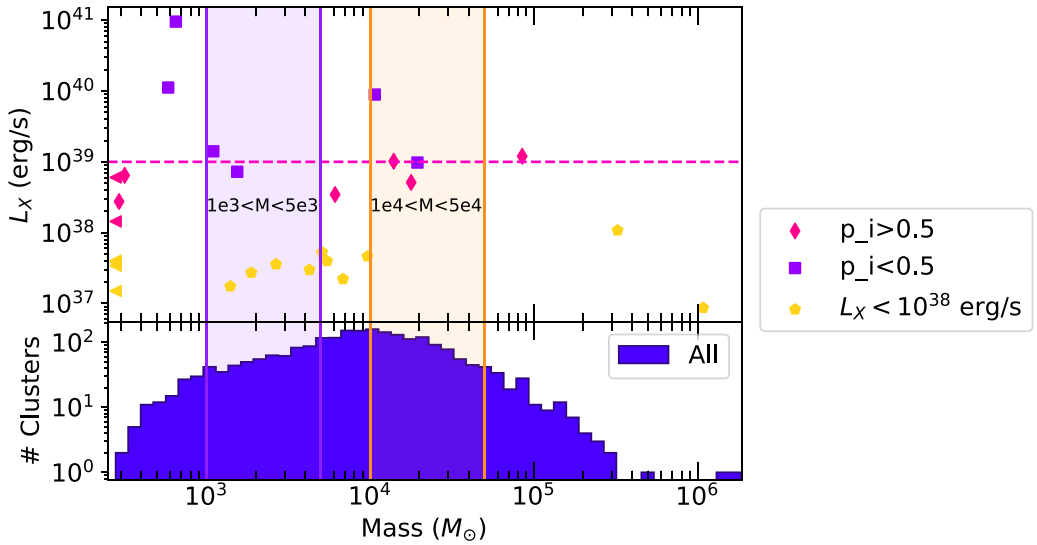

Figure 3. X-ray luminosity vs. masses of cluster candidates. The upper panel shows the estimated mass of the cluster candidates vs. the X-ray luminosity. The lower panel shows a histogram of the mass estimates for all of the cluster candidates (with contaminants removed), and we have shaded in regions of clusters with masses between 1000 and 5000 $M_\odot$ as well as 10,000 and 50,000 $M_\odot$ to better compare to U. N. Di Carlo et al. (2021).

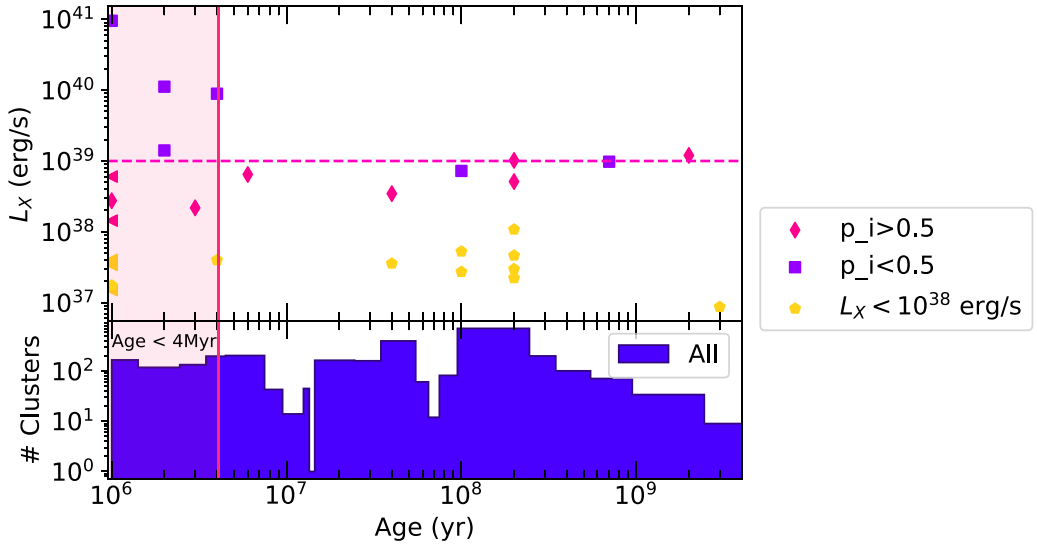

Figure 4. X-ray luminosity vs. ages of cluster candidates. The upper panel shows the estimated age of the cluster candidates vs. the 0.3–10 keV X-ray luminosity. The lower panel shows a histogram of the age estimates for all of the cluster candidates (with contaminants removed). For visualization purposes, we have shaded in ages of less than 4 Myr, where it is possible that enough ICM may be present for a BH to accrete without a companion.

above 1000 $M_\odot$ are src31 and src36. Both have X-ray luminosities above 10^{39} erg s^{-1}, low-probability matches (25% and 12%, respectively), and the matches with similar probabilities are class 4 contaminants. Therefore, it is quite unlikely that either of these sources is associated with the nearby star cluster.

3.1. Comparison to Star Cluster Simulations

While it is nontrivial to compare observations to theory, due to the number of difficulties in interpreting the nature of the X-ray sources, given the wealth of theory, we naively make an attempt to reconcile our observations with current predictions by simulations. For example, S. F. Portegies Zwart et al. (2004) show how massive BHs can form via runaway collisions in a young cluster.

In newer simulations by U. N. Di Carlo et al. (2021), the most massive BH formed is just under 500 $M_\odot$ in a low-metallicity cluster, with the majority of IMBHs having masses between 100 $M_\odot$ and 200 $M_\odot$, although these results are sensitive to the initial conditions of the simulation. They found that under 1% of star clusters with masses between 1000 and 5000 $M_\odot$ form an IMBH, but 8% of star clusters with masses between 10^4 $M_\odot$ and 5×10^4 $M_\odot$ produce an IMBH. For the lowest-mass clusters, S. Rastello et al. (2021) find that up to 85% of the IMBHs are ejected from the parent cluster. S. Torniamenti et al. (2022) find that for clusters with masses between 500 and 800 $M_\odot$, less than 0.01% of the BHs they form are still bound to their low-mass parent cluster.

One of the major challenges of comparing X-ray observations of potential BHs to theory is not knowing how many of the IMBHs predicted from the simulations will be accreting from a stellar companion and thus producing observable X-rays. However, if the ICM is dense enough for the BH to accrete from, we might expect to see more X-ray sources

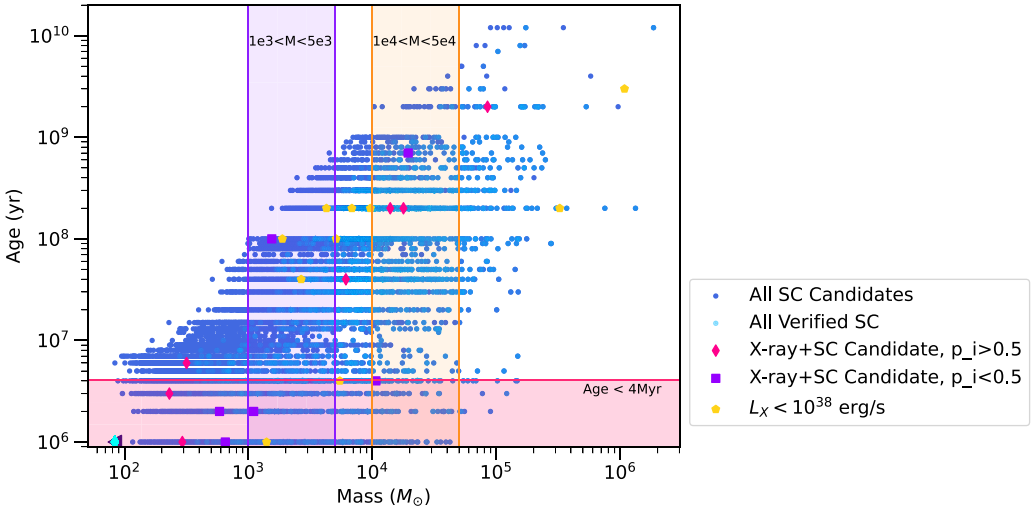

Figure 5. Mass vs. age estimates of all the LEGUS star cluster candidates (with class 4 objects removed). Verified star clusters are overlaid in a lighter color. The solid pink diamonds represent the properties of the star cluster candidates with high-probability (>50%) matches, and the purple squares represent the star cluster candidates with low-probability (<50%) matches. The yellow pentagons are the $L_X < 10^{38}$ erg s^{-1} sources, which are all higher-probability matches to candidate star clusters (p_i > 50%). We highlight the same regions of interest as before, with ages less than 4 Myr and cluster masses between 1000 and 5000 $M_\odot$ as well as between 10,000 and 50,000 $M_\odot$.

produced by clusters with ages less than 4 Myr. We therefore separate out clusters with ages of less than 4 Myr and assess whether they host more X-ray sources than the older clusters.

For star clusters with ages <4 Myr, there are almost 800 star clusters in the 500–800 $M_\odot$ mass range, just under 1000 with masses in the 1000–5000 $M_\odot$ mass range (Figure 5), with ~130 clusters falling into the 1×10^4–5×10^4 $M_\odot$ mass range. If we assume that IMBHs in clusters with ages <4 Myr can efficiently accrete off of the ICM and produce X-rays above some amount, we might expect to see 10 X-ray sources (1%) in the 1000–5000 $M_\odot$ mass range and a further 10 (8%) in the 1×10^4–5×10^4 $M_\odot$ mass range. We see no bright X-ray sources with high-probability matches and ages less than 4 Myr in these mass ranges, and two low-probability matches. Our search for X-ray-faint sources in the longest observations (Table 3) yielded three high-probability matches with L_X between 9×10^{36} and 2×10^{37} erg s^{-1} to clusters with ages less than 4 Myr and masses between 500 $M_\odot$ and 5000 $M_\odot$.

3.2. Implications of Radio Observations

Our limiting 10 GHz radio luminosity is ~10^{34} erg s^{-1}. If we assume a point source with a flat spectrum, then the 5 GHz limiting radio luminosity is 7×10^{33} erg s^{-1}. Using the assumptions of the fundamental plane and Equation (8) from K. Gültekin et al. (2019), our current radio sensitivity limits mean that we are only able to detect radio emission from IMBHs with masses 10^4 $M_\odot$ or above. This is sensible: Figure 6 shows IMBHs with masses below 10^3 $M_\odot$ will not have low-efficiency accretion for the very brightest X-rays (10^{38} erg s^{-1} or above), where we would expect to see radio.

With the advent of next-generation radio facilities, like the next-generation VLA,[19] we can push the limiting radio luminosities down to 7×10^{32} erg s^{-1}, which corresponds to an increased sensitivity to BHs of masses down to 10^3 $M_\odot$. Our estimates for the detection of IMBHs at 10 Mpc are roughly consistent with the estimates of radio emission from IMBHs at 17 Mpc by J. M. Wrobel et al. (2021). This is also true for the Square Kilometre Array (SKA); the most recent version of the SKA Mid sensitivity calculator[20] suggests that a 1 hr exposure will produce a limiting rms of 550 nJy. Our estimates are consistent with similar estimates for IMBHs at 20 Mpc by B. Karimi et al. (2024).

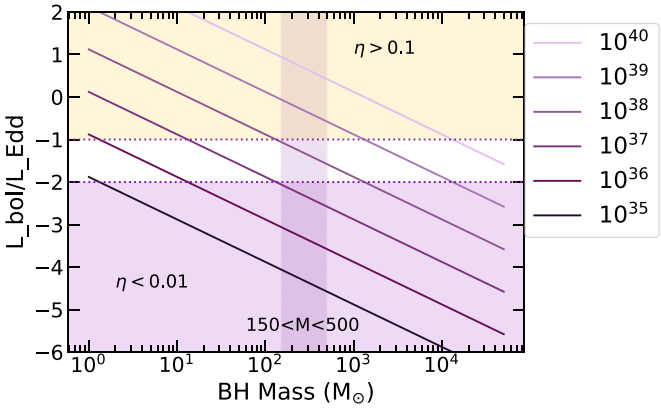

Figure 6. Accretion efficiency for BHs from 1 $M_\odot$ to 5×10^4 $M_\odot$, with a range of X-ray luminosities from 10^{35} to 10^{40} erg s^{-1}. If η is below 0.01, then the assumptions of the fundamental plane hold, and one can expect radio emission from the source. If η is above 0.1, then the source is expected to be in the super-Eddington state.

3.3. Speculation on Detectability of Accreting IMBHs in YMCs

While it is very difficult to interpret the nature of the X-ray sources in the absence of radio detections, we can explore the nature of the X-ray emissions from M51's star clusters and if any at all are likely to be IMBHs. We first note that the X-rays of the luminosities we discuss here can be produced by a multitude of objects: IMBHs accreting under the assumptions of the fundamental plane, low-luminosity accretion from an IMBH, or super-Eddington accretion from a stellar-mass BH or neutron star.

[19] https://ngect.nrao.edu/

[20] https://sensitivity-calculator.skao.int/mid

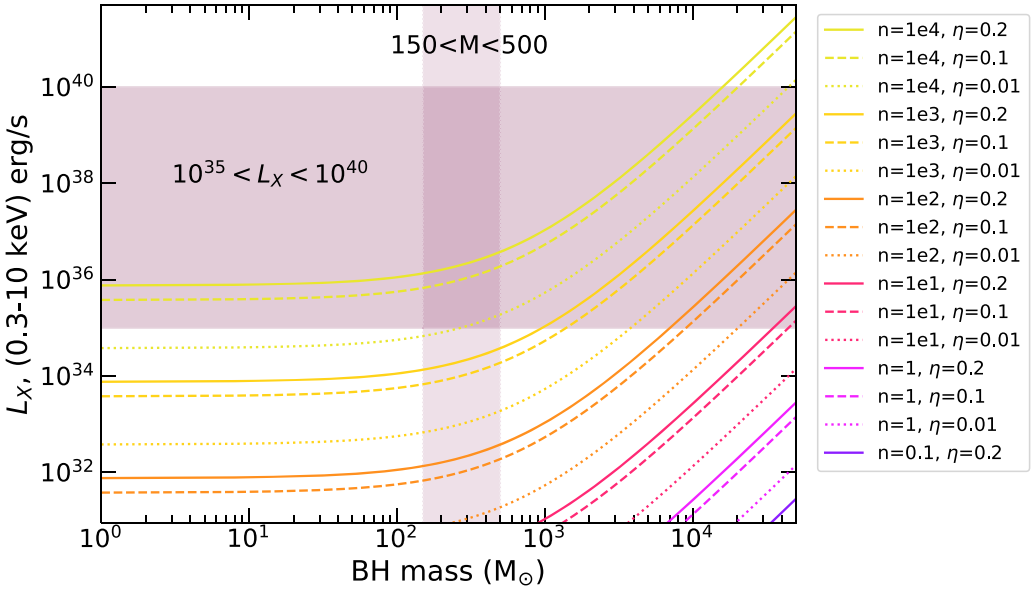

Figure 7. Predicted X-ray luminosity for embedded gases of different densities (from $n = 0.1$, which is more typical of an older globular cluster, to $n = 10^4$ cm^{-3}) and different accretion efficiencies (1%, 10%, and 20%), assuming Bondi–Hoyle–Littleton accretion. At the distance of M51, unless the gas is extremely dense (10^4 cm^{-3}), detecting IMBHs with mass less than $10^3\ M_\odot$ in X-ray is difficult. For BHs with mass $> 10^3\ M_\odot$, densities above 1 can be observable in X-ray, but we would only expect radio emission in the cases with 1% accretion efficiency, which would require either the higher density (10^4 cm^{-3}) or a BH more massive than $5 \times 10^4\ M_\odot$.

We attempt to discriminate between these scenarios, but acknowledge that in the absence of a secure radio detection that can be linked to the X-ray using the fundamental plane, it is impossible to truly classify the nature of the compact object. F. Fortin et al. (2023, 2024) show that no LMXRBs persistently exceed 10^{38} erg s^{-1} in our Galaxy and only three HMXRBs exceed 10^{38} erg s^{-1}. Indeed, the HMXRB X-ray luminosity function (XLF) clearly peaks below 10^{36} erg s^{-1}. We know that the XLF varies depending on Galaxy type and that ULXs with both high- and low-mass companion stars can be observed outside the Milky Way (B. D. Lehmer et al. 2014; M. B. Peacock & S. E. Zepf 2016), but this already highlights the unique nature of these X-ray-bright sources, whether they are IMBHs or stellar-mass compact objects. While we cannot appeal to our understanding of Milky Way–bright X-ray sources to help us interpret those found in M51, we can make some naive speculations to try to better align IMBH predictions from theory and what we are able to observe.

Given the current observational constraints, what does observing an IMBH look like in star clusters at M51's distance? There are roughly 2500 star clusters in M51 with masses between $10^4\ M_\odot$ and $5 \times 10^4\ M_\odot$. If up to 8% of these clusters can host IMBHs, that translates to 200 possible IMBHs. Not all of these are necessarily in a binary accreting at high enough rates to produce observable X-rays at the distance of M51. Currently, we see two high-probability X-ray sources with $L_X > 10^{35}$ erg s^{-1} matching to clusters that match this criterion, which means that if both of these are IMBHs, then only 1% of these IMBHs can be detected in X-ray in present-day clusters.

However, in the case of clusters with ages less than 4 Myr, it may be possible that there is enough intercluster medium and winds from supergiant stars that have not yet been swept out. Figure 7 shows the predicted X-ray luminosities for Bondi–Hoyle–Littleton accretion for a range of BH masses. We follow the same assumptions as A. Paduano et al. (2024), except that while they fix the number density to 0.2 for globular clusters, we test it for a range of densities, from 0.01 to 10^4 cm^{-3}. This is only a simplistic assessment, and we refer the reader to X.-Q. Han et al. (2021) for more complicated interactions, like irradiation-driven winds.

For BHs in the mass range of 150–500 $M_\odot$, we will be able to detect them in X-ray at these distances if they are accreting from the ICM with a number density of 10^4 cm^{-3}. For more massive BHs, we can start detecting them in X-ray at the distance of M51 with lower densities, but the ones that have radiatively inefficient accretion will be toward the tail end of the X-ray luminosities we are sensitive to and not necessarily detected in radio. For these young regions, 1–10^3 cm^{-3} are reasonable densities to expect in H II regions, based on those observed in the LMC and SMC (L. A. Lopez et al. 2014). Higher densities are observed in the ultracompact H II regions, but this phase is short-lived (<1 Myr; E. Churchwell 2002). There may be other contributions to increasing the number density of the ICM via wind loss through massive stars in the cluster (W. Chantereau et al. 2020), which would lead toward being able to detect BHs less massive than $10^3\ M_\odot$ in X-ray, if not in radio.

BHs with masses well above $10^4\ M_\odot$ are unlikely to form in these cluster systems (M. Mapelli et al. 2012). Even if they were likely to form, detecting them would be challenging. As discussed previously, if the $10^4\ M_\odot$ IMBH could form at a young enough age to be embedded in an intercluster medium (<4 Myr), then accretion from the dense gas could give rise to X-ray and radio emission detectable with current facilities.

Accretion by a $\sim 10^4\ M_\odot$ IMBH is known to generate X-ray and compact radio emission, as in the case of the IMBH candidate HLX-1, a hyperluminous X-ray source with observed spectral state transitions reminiscent of BH binaries (N. Webb et al. 2012). The known episodic ejections produced during the high X-ray state in XRBs were observed in HLX-1, although detection in this ejection phase as depicted in the fundamental plane relation is known to be relatively difficult for IMBHs (X. Yang & J. Yang 2023).

A tidal disruption event (TDE) by an IMBH may be another possibility for explaining the X-ray emission we see. Depending on the assumptions made in the evolution of TDE modeling, accretion onto the disk can remain at a fallback rate that is still super-Eddington at late times, in some cases up to a few to tens of years from the initial disruption (V. L. Tang et al. 2024). In this phase, the bulk of the disk emission occurs in the soft X-rays. Very late-rising radio-luminous TDEs have been observed, but only for higher BH masses, as in the case of F. Zhang et al. (2024), where a late-rising radio emission preceded the decay of the optical light curve with a delayed soft-X-ray flare. In fact, Y. Cendes et al. (2024) found that 40% of all optical TDEs are detected in radio hundreds to thousands of days after discovery. Though these TDEs are due to BHs of a few orders of magnitude beyond the BH masses considered for star clusters, it may nonetheless be worth noting that while such TDEs are possible perhaps at lower BH masses, no unambiguous radio emissions due to a TDE by an IMBH of $\sim 10^4\ M_\odot$ have been reported. Furthermore, the predicted disruption rates of TDEs are generally quite low and can vary up to a few factors, due to the considerable uncertainties in the modeling of TDEs around IMBHs (e.g., F. P. Rizzuto et al. 2023; V. L. Tang et al. 2024), and depend sensitively on the stellar distribution around the BH set by the relaxation timescale. For low-density stellar environments, relaxation takes longer, and the continued supply of stars into the lost-cone orbits required for disruptions is therefore less frequent, and thus the TDE rate is much lower.

In this case, we are unlikely to be sensitive to tidally disrupting IMBHs, because these events are extremely rare and the observing cadence of Chandra is unlikely to constrain signatures of TDEs in X-ray.

4. Summary and Conclusions

We have leveraged existing star cluster catalogs from LEGUS and archival X-ray observations from Chandra to search for bright X-ray point sources associated with or possibly hosted by star clusters, using a Bayesian cross-matching algorithm. We performed model fitting of the HST observations to classify the cluster candidates based on their structural parameters and found that 17 of the brightest X-ray sources likely matched to a cluster candidate, with 11 having greater than a 50% probability of matching. Fourteen of the lower-luminosity sources were high-probability matches to a star cluster candidate.

We compared the X-ray luminosity to the age and mass estimates for the clusters and found that the majority of the X-ray sources were affiliated with young low-mass clusters. We searched for potential radio counterparts to these and did not find any emission above a radio luminosity of 10^{34} erg s^{-1} at 10 GHz, except for Src03, which had a 70 μJy radio counterpart at 10 GHz. This radio counterpart was also detected by L. A. Maddox et al. (2007), who classify it as a compact Hα source. Because the X-ray spectrum of Src03 is soft (T. Sanatombi et al. 2023), we thus do not find that the radio emission could be suggestive of an IMBH under the assumptions of the fundamental plane.

We made some initial comparisons to predictions from simulations and found that for star clusters with masses between $10^4\ M_\odot$ and $5 \times 10^4\ M_\odot$, only four at most matched to the brightest X-ray sources (i.e., those most likely to be IMBHs), with two being low-probability matches. For the 2500 clusters in this mass range, theory predicts that 8% or 200 should have IMBHs at some point in their lifetime. This discrepancy implies that only a very low fraction of IMBHs could be producing X-ray emission detectable at the distance of M51.

Although, with X-ray detections alone, we cannot distinguish XRBs and ULXs with a stellar-mass compact object from a bona fide IMBH, we speculate on the observability of IMBHs in both X-rays and radio, at the distance of M51. For clusters with ages <4 Myr, it is possible that a massive IMBH could produce sufficient X-ray emission to be observed from only the ICM and in the absence of a companion star. While we would not be sensitive to any radio emission from BHs $\lesssim 10^4\ M_\odot$ under these conditions, next-generation radio facilities like the SKA and the next-generation VLA would be able to detect radio emission from BHs $\gtrsim 10^3\ M_\odot$.

Acknowledgments

We thank the referee for helpful comments that greatly improved the manuscript. The authors thank Jillian Bellovary, Rupali Chandar, Angiraben Mahida, and Michela Mapelli for helpful discussion. K.C.D. acknowledges the support for this work provided by NASA through the NASA Hubble Fellowship grant HST-HF2-51528 awarded by the Space Telescope Science Institute, which is operated by the Association of Universities for Research in Astronomy, Inc., for NASA, under contract NAS5-26555. E.W.K. acknowledges the support from the Smithsonian Institution as a Submillimeter Array (SMA) Fellow.

Facilities: VLA, HST, CXO.

Software: astropy (Astropy Collaboration et al. 2013), CASA (CASA Team et al. 2022), matplotlib (J. D. Hunter 2007), NumPy (C. R. Harris et al. 2020), pandas (W. McKinney 2010), NWAY (M. Salvato et al. 2018), CIAO (A. Fruscione et al. 2006).

ORCID iDs

Kristen C. Dage https://orcid.org/0000-0002-8532-4025
Evangelia Tremou https://orcid.org/0000-0002-4039-6703
Bolivia Cuevas Otahola https://orcid.org/0000-0002-1046-1500
Eric W. Koch https://orcid.org/0000-0001-9605-780X
Kwangmin Oh https://orcid.org/0000-0003-1814-8620
Richard M. Plotkin https://orcid.org/0000-0002-7092-0326
Vivian L. Tang https://orcid.org/0009-0003-7709-5474
Muhammad Ridha Aldhalemi https://orcid.org/0009-0004-9310-020X
Zainab Bustani https://orcid.org/0009-0006-8696-9892
Mariam Ismail Fawaz https://orcid.org/0009-0005-2051-1304
Hans J. Harff https://orcid.org/0009-0006-5976-8120
Amna Khalyleh https://orcid.org/0009-0000-6403-8903
Timothy McBride https://orcid.org/0009-0007-9611-1774
Jesse Mason https://orcid.org/0009-0006-2324-0738
Anthony Preston https://orcid.org/0009-0000-8689-3476
Cortney Rinehart https://orcid.org/0009-0001-7561-6753
Ethan Vinson https://orcid.org/0009-0003-1543-4514
Gemma Anderson https://orcid.org/0000-0001-6544-8007
Edward M. Cackett https://orcid.org/0000-0002-8294-9281
Shih Ching Fu https://orcid.org/0000-0002-9077-6026
Sebastian Kamann https://orcid.org/0000-0001-6604-0505
Teresa Panurach https://orcid.org/0000-0001-8424-2848

Renuka Pechetti https://orcid.org/0000-0002-1670-0808
Payaswini Saikia https://orcid.org/0000-0002-5319-6620
Susmita Sett https://orcid.org/0000-0001-9261-1738
Ryan Urquhart https://orcid.org/0000-0003-1814-8620
Christopher Usher https://orcid.org/0000-0002-7383-7106

References

Abolmasov, P. K., Swartz, D. A., Fabrika, S., et al. 2007, ApJ, 668, 124
Adamo, A., Ryon, J. E., Messa, M., et al. 2017, ApJ, 841, 131
Akyuz, A., Akkaya Oralhan, I., Allak, S., et al. 2024, MNRAS, 529, 1507
Askar, A., Baldassare, V. F., & Mezcua, M. 2023, arXiv:2311.12118
Astropy Collaboration, Robitaille, T. P., Tollerud, E. J., et al. 2013, A&A, 558, A33
Atapin, K., Vinokurov, A., Sarkisyan, A., et al. 2024, MNRAS, 527, 10185
Avdan, H., Avdan, S., Akyuz, A., et al. 2016, ApJ, 828, 105
Bachetti, M., Harrison, F. A., Walton, D. J., et al. 2014, Natur, 514, 202
Bañados, E., Venemans, B. P., Mazzucchelli, C., et al. 2018, Natur, 553, 473
Bastian, N., & Strader, J. 2014, MNRAS, 443, 3594
Binder, B. A., Anderson, A. K., Garofali, K., Lazzarini, M., & Williams, B. F. 2023, MNRAS, 522, 5669
Briggs, D. S. 1995, AAS Meeting Abstracts, 187, 112.02
Cabrera-Ziri, I., Bastian, N., Longmore, S. N., et al. 2015, MNRAS, 448, 2224
Calzetti, D., Lee, J. C., Sabbi, E., et al. 2015, AJ, 149, 51
CASA Team, Bean, B., Bhatnagar, S., et al. 2022, PASP, 134, 114501
Cendes, Y., Berger, E., Alexander, K. D., et al. 2024, ApJ, 971, 185
Chantereau, W., Biernacki, P., Martig, M., et al. 2020, MNRAS, 493, 1306
Churchwell, E. 2002, ARA&A, 40, 27
Cuevas-Otahola, B., Mayya, Y. D., Puerari, I., & Rosa-González, D. 2022, PASP, 134, 024502
Dage, K. C., Zepf, S. E., Thygesen, E., et al. 2020, MNRAS, 497, 596
Di Carlo, U. N., Giacobbo, N., Mapelli, M., et al. 2019, MNRAS, 487, 2947
Di Carlo, U. N., Mapelli, M., Pasquato, M., et al. 2021, MNRAS, 507, 5132
Elson, R. A. W., Fall, S. M., & Freeman, K. C. 1987, ApJ, 323, 54
Evans, I. N., Primini, F. A., Glotfelty, K. J., et al. 2010, ApJS, 189, 37
Fabbiano, G. 1989, ARA&A, 27, 87
Falcke, H., Körding, E., & Markoff, S. 2004, A&A, 414, 895
Fortin, F., Garcìa, F., Simaz Bunzel, A., & Chaty, S. 2023, A&A, 671, A149
Fortin, F., Kalsi, A., Garcìa, F., Simaz-Bunzel, A., & Chaty, S. 2024, A&A, 684, A124
Freire, P. C., Kramer, M., Lyne, A. G., et al. 2001, ApJL, 557, L105
Fruscione, A., McDowell, J. C., Allen, G. E., et al. 2006, Proc. SPIE, 6270, 62701V
Gladstone, J. C., Roberts, T. P., & Done, C. 2009, MNRAS, 397, 1836
Greene, J. E., Strader, J., & Ho, L. C. 2020, ARA&A, 58, 257
Gültekin, K., King, A. L., Cackett, E. M., et al. 2019, ApJ, 871, 80
Häberle, M., Neumayer, N., Seth, A., et al. 2024, Natur, 631, 285
Han, X.-Q., Jiang, L., & Chen, W.-C. 2021, ApJ, 914, 109
Hannon, S., Lee, J. C., Whitmore, B. C., et al. 2019, MNRAS, 490, 4648
Harris, C. R., Millman, K. J., Millman, K. J., van der Walt, S. J., et al. 2020, Natur, 585, 357
Heida, M., Jonker, P. G., Torres, M. A. P., et al. 2014, MNRAS, 442, 1054
Ho, L. C. 2008, ARA&A, 46, 475
Hollyhead, K., Bastian, N., Adamo, A., et al. 2015, MNRAS, 449, 1106
Hunt, Q., Chandar, R., Gallo, E., et al. 2023, ApJ, 953, 126
Hunter, J. D. 2007, CSE, 9, 90
Karimi, B., Barmby, P., & Abbassi, S. 2024, ApJ, 974, 260
King, I. R. 1966, AJ, 71, 64
Kovlakas, K., Zezas, A., Andrews, J. J., et al. 2020, MNRAS, 498, 4790
Lehmer, B. D., Berkeley, M., Zezas, A., et al. 2014, ApJ, 789, 52
Leitherer, C., Schaerer, D., Goldader, J. D., et al. 1999, ApJS, 123, 3
López, K. M., Heida, M., Jonker, P. G., et al. 2017, MNRAS, 469, 671
Lopez, L. A., Krumholz, M. R., Bolatto, A. D., et al. 2014, ApJ, 795, 121
Maddox, L. A., Cowan, J. J., Kilgard, R. E., Schinnerer, E., & Stockdale, C. J. 2007, AJ, 133, 2559
Mapelli, M., Moore, B., Giordano, L., et al. 2008, MNRAS, 383, 230
Mapelli, M., & Zampieri, L. 2014, ApJ, 794, 7
Mapelli, M., Zampieri, L., & Mayer, L. 2012, MNRAS, 423, 1309
McKinney, W. 2010, in Proc. 9th Python in Science Conf., ed. S. van der Walt & J. Millman (Austin, TX: SciPy), 56
McMullin, J. P., Waters, B., Schiebel, D., Young, W., & Golap, K. 2007, in ASP Conf. Ser. 376, Astronomical Data Analysis Software and Systems XVI, ed. R. A. Shaw, F. Hill, & D. J. Bell (San Francisco, CA: ASP), 127
McQuinn, K. B. W., Skillman, E. D., Dolphin, A. E., Berg, D., & Kennicutt, R. 2016, ApJ, 826, 21
Merloni, A., Heinz, S., & di Matteo, T. 2003, MNRAS, 345, 1057
Mezcua, M., Roberts, T. P., Lobanov, A. P., & Sutton, A. D. 2015, MNRAS, 448, 1893
Mezcua, M., Roberts, T. P., Sutton, A. D., & Lobanov, A. P. 2013, MNRAS, 436, 3128
Paduano, A., Bahramian, A., Miller-Jones, J. C. A., et al. 2024, ApJ, 961, 54
Panurach, T., Dage, K. C., Urquhart, R., et al. 2024, ApJ, 977, 211
Peacock, M. B., & Zepf, S. E. 2016, ApJ, 818, 33
Pechetti, R., Seth, A., Kamann, S., et al. 2022, ApJ, 924, 48
Perley, R. A., Chandler, C. J., Butler, B. J., & Wrobel, J. M. 2011, ApJL, 739, L1
Pike, S. N., Harrison, F. A., Bachetti, M., et al. 2019, ApJ, 875, 144
Portegies Zwart, S. F., Baumgardt, H., Hut, P., Makino, J., & McMillan, S. L. W. 2004, Natur, 428, 724
Portegies Zwart, S. F., & McMillan, S. L. W. 2002, ApJ, 576, 899
Portegies Zwart, S. F., McMillan, S. L. W., & Gieles, M. 2010, ARA&A, 48, 431
Rangelov, B., Chandar, R., Prestwich, A., & Whitmore, B. C. 2012, ApJ, 758, 99
Rangelov, B., Prestwich, A. H., & Chandar, R. 2011, ApJ, 741, 86
Rastello, S., Mapelli, M., Di Carlo, U. N., et al. 2021, MNRAS, 507, 3612
Rau, U. 2012, Proc. SPIE, 8500, 85000N
Rizzuto, F. P., Naab, T., Rantala, A., et al. 2023, MNRAS, 521, 2930
Rodrìguez, M. J., Lee, J. C., Whitmore, B. C., et al. 2023, ApJL, 944, L26
Rodrìguez Castillo, G. A., Israel, G. L., Belfiore, A., et al. 2020, ApJ, 895, 60
Saikia, P., Körding, E., Coppejans, D. L., et al. 2018, A&A, 616, A152
Saikia, P., Körding, E., & Falcke, H. 2015, MNRAS, 450, 2317
Salvato, M., Buchner, J., Budavári, T., et al. 2018, MNRAS, 473, 4937
Sanatombi, T., Devi, A. S., & Singh, K. Y. 2023, ChJPh, 83, 579
Tang, V. L., Madau, P., Bortolas, E., et al. 2024, ApJ, 963, 146
Terashima, Y., Inoue, H., & Wilson, A. S. 2006, ApJ, 645, 264
Torniamenti, S., Rastello, S., Mapelli, M., et al. 2022, MNRAS, 517, 2953
Tremou, E., Strader, J., Chomiuk, L., et al. 2018, ApJ, 862, 16
Urquhart, R., Soria, R., Johnston, H. M., et al. 2018, MNRAS, 475, 3561
Vázquez, G. A., & Leitherer, C. 2005, ApJ, 621, 695
Webb, N., Cseh, D., Lenc, E., et al. 2012, Sci, 337, 554
Weisskopf, M. C., Brinkman, B., Canizares, C., et al. 2002, PASP, 114, 1
Wilson, C. P. 1975, AJ, 80, 175
Wrobel, J. M., Maccarone, T. J., Miller-Jones, J. C. A., & Nyland, K. E. 2021, ApJ, 918, 18
Yang, X., & Yang, J. 2023, Galax, 11, 53
Yu, H., Zhu, M., Xu, J.-L., et al. 2023, MNRAS, 521, 2719
Zhang, F., Shu, X., Yang, L., et al. 2024, ApJL, 962, L18